Correlation of Atomic Structure and Photoluminescence of the Same Quantum Dot: Pinpointing Surface and Internal Defects That Inhibit Photoluminescence

Noah J. Orfield,[†,‡] James R. McBride,[*,†,‡] Joseph D. Keene,[†,‡] Lloyd M. Davis,[§,∥] and Sandra J. Rosenthal[*,†,‡,§,∥,⊥,#,▽,⊗]

[†]Department of Chemistry, Vanderbilt University, Nashville, Tennessee 37235, United States, [‡]Vanderbilt Institute for Nanoscale Science and Engineering, Vanderbilt University, Nashville, Tennessee 37235, United States, [§]Department of Physics and Astronomy, University of Tennessee Knoxville, Knoxville, Tennessee 37996, United States, [∥]Center for Laser Applications, University of Tennessee Space Institute, Tullahoma, Tennessee 37388, United States, [⊥]Department of Interdisciplinary Materials Science, Vanderbilt University, Nashville, Tennessee 37235, United States, [#]Department of Physics and Astronomy, Vanderbilt University, Nashville, Tennessee 37235, United States, [▽]Department of Pharmacology, Chemical and Biomolecular Engineering, Vanderbilt University, Nashville, Tennessee 37235, United States, and [⊗]Materials Science and Technology Division, Oak Ridge National Laboratory, Oak Ridge, Tennessee 37831, United States

ABSTRACT In a size regime where every atom counts, rational design and synthesis of optimal nanostructures demands direct interrogation of the effects of structural divergence of individuals on the ensemble-averaged property. To this end, we have explored the structure—function relationship of single quantum dots (QDs) *via* precise observation of the impact of atomic arrangement on QD fluorescence. Utilizing wide-field fluorescence microscopy and atomic number contrast scanning transmission electron microscopy (Z-STEM), we have achieved correlation of photoluminescence (PL) data and atomic-level structural information from individual colloidal QDs. This investigation of CdSe/CdS core/shell QDs has enabled exploration of the fine structural factors necessary to control QD PL. Additionally, we have identified specific morphological and structural anomalies, in the form of internal and surface defects, that consistently vitiate QD PL.

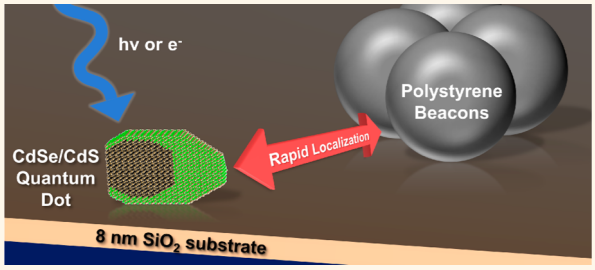

KEYWORDS: nanocrystal quantum dots · core/shell quantum dots · semiconductor nanocrystals · single nanocrystal microscopy · single nanocrystal spectroscopy · nanocrystal atomic structure · correlation

Semiconductor QDs hold great promise for implementation in energy-efficient devices due to their high quantum yields, large extinction coefficients, and a high level of synthetic control over absorption, emission and electroluminescence properties.[1] Recent advances have resulted in realization of colloidal QD-based devices including light emitting diodes (LEDs),[2−4] flexible LED displays,[5] photovoltaics,[6] solar concentrators,[7] QD-lasers,[8] and even widespread use of QDs as a diffuser in LED displays.[9] Further, QDs have reached ubiquity as molecular probes for *in vitro* fluorescence imaging because of their limited photobleaching, which enables robust fluorescence labeling and single particle tracking.[10] Despite their potential, colloidal QDs are plagued with charging and nonradiative recombination, phenomena which can be probed *via* time-resolved single QD spectroscopy and are manifested in the PL intermittency (PI) characteristic of single QDs.[11−14]

Since the first report on nanocrystal PI in 1996,[11] a large number of studies have investigated this phenomenon, which gives rise to an "off" time probability distribution governed by inverse power law statistics. These studies have shown that PI seems to arise due to trapping of charge carriers either within or at the surface of the QD heterostructure, and subsequent nonradiative recombinations within the charged QD.[15,16] Prior comprehensive studies have

* Address correspondence to james.r.mcbride@vanderbilt.edu, sandra.j.rosenthal@vanderbilt.edu.

Received for review November 10, 2014 and accepted December 18, 2014.

Published online December 18, 2014
10.1021/nn506420w

© 2014 American Chemical Society

determined the dependency of "on"/"off" probability distributions on such factors as excitation intensity, excitation wavelength, and, when considering core/shell QDs, shell composition and thickness.[17−20]

There are many variations of core/shell syntheses in the literature, with variance in both the shell composition[21] and the level of gradation between core and shell.[22] Development of nonblinking QDs has been achieved by multiple groups; this blinking suppression is accomplished by encapsulating cores with many layers of shell material[23] and/or alloying materials to yield a smooth chemical potential between the core and shell.[24,25] Even these syntheses, however, produce a fraction of QDs that do not exhibit blinking suppression or are permanently dark, presumably due to structural inhomogeneity.[26] QD-to-QD structural variance almost certainly accounts for inhomogeneity noted in biexciton quantum yield, a parameter that must be optimized for realization of efficient QD lasers.[27] In other cases, QD blinking is actually desirable—superresolution microscopy (nanoscopy) is attainable when the implemented fluorescent species exhibits fast photoswitching, thereby facilitating localization of single fluorophores separated by nanometer distances.[28,29]

Previous attempts at correlating single QD structural information *via* electron microscopy with fluorescence data have been difficult.[30,31] These studies reported ambiguity in the correlation method that inhibited the ability to collect data from a large sample of the representative QD population. Implementation of atomic force microscopy (AFM) in conjunction with optical microscopy fails to provide structural insights at the atomic level. As a result, large-scale single-QD PL studies have frequently treated all QDs as structurally identical. Detailed investigation of the shape, size and structure of QDs, however, reveals appreciable heterogeneity among individuals from the same batch.[32] Indeed, inhomogeneous broadening in the PL spectra of ensemble QDs is a well-known phenomenon,[33] and has been attributed to the native polydispersity of colloidal QD samples.[34] Adding another degree of complexity, core/shell syntheses result in a complex atomic landscape with unique inorganic junctions on each QD; this landscape affects the excitation dynamics, decay dynamics, oscillator strength, and multiexciton properties,[25] which fluctuate with the addition of even a single atomic layer of core or shell material. In turn, the macroscopic properties of a group of these unique emitters are highly dependent on the distribution of atomic and electronic properties of QDs in the ensemble. Therefore, in order to fully comprehend the effects of atomistic structural variance on the electronic structure as a part of the ongoing effort to achieve complete control over QD fluorescence, correlation of structural information with collected PL transients for individual QDs is imperative.[35−38] Our highly reproducible and unambiguous correlation methodology meets this need.

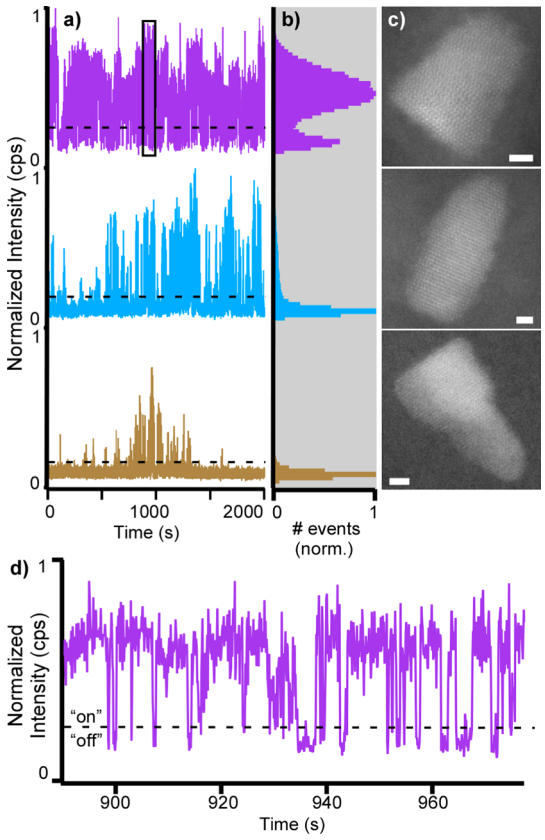

Figure 1. Correlated fluorescence and structural data for individual QDs. Shown in (a) are full fluorescence intensity transients; (b) shows the corresponding fluorescence intensity histograms for the 3 QDs whose structures are shown in (c). (d) The boxed truncated portion of the topmost fluorescence intensity transient in (a) shows the "on" and "off" states of a fluorescent QD. Scale bars in (c) are 2 nm.

RESULTS AND DISCUSSION

Correlation of Atomic Structure and Photoluminescence of Single Quantum Dots. For this study, PL time traces and high angle annular dark field (HAADF), also known as atomic number contrast scanning transmission electron microscopy (Z-STEM), images were collected for a total of 84 QDs, examples of which are shown in Figure 1.

For our experiments, we chose to use commercial QDs (Life Technologies, QDOT 655). In ensemble, these QDs possess a narrow emission fwhm of 27 nm; the typical morphology and detailed atomic structure have also been described in the past.[32] Despite the high quality of the ensemble optical spectra, the aforementioned previous studies showed that a moderate level of structural and morphological diversity is encountered on a single QD basis. This QD-to-QD variation provides an ideal platform from which we can learn about both core/shell growth phenomena and structure−function relationships of QD heterostructures. The ensemble statistics of the 84 QDs studied are highlighted in Figure 2.

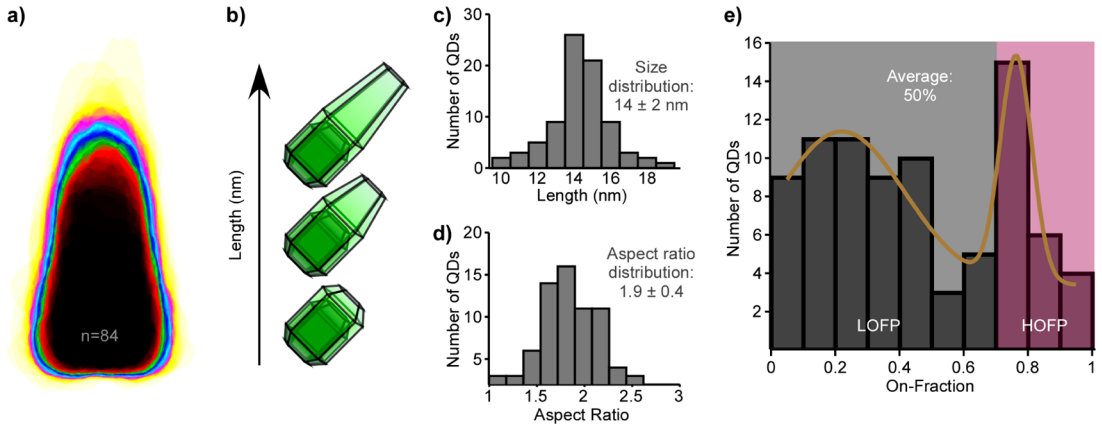

Figure 2. Heterogeneity within the core/shell nanocrystal ensemble. (a) A heat map overlay of the 84 QDs investigated displays the morphological heterogeneity in the observed population. (b) Because the core size is effectively equal among QDs, length reflects the amount of shell coverage in the direction of the C_{3v} (long) axis. (c) Size distribution and (d) aspect ratio distribution of the examined QD population. (e) The distribution of all observed QDs as a function of on-fraction. We observed that the QDs inhabited a low on-fraction population (LOFP) and high on-fraction population (HOFP).

The heat map overlay shown in Figure 2a illustrates the physical heterogeneity of the QDs studied here. The morphology studied is an anisotropic core/shell, with the CdSe core in the dark region of the heat map and the CdS shell growing preferentially in a lengthwise direction. Heterodispersity observed in the length of these QDs is reflective of differing amounts of shell material, as illustrated in Figure 2b and shown in the histograms in Figure 2c,d.

For each QD, the amount of time spent in the emissive "on" state was calculated and divided by the total collection time to find the QD on-fraction.[39] All on-fraction data is represented in the histogram shown in Figure 2e. All of the QDs examined, including the 7 permanently nonradiative QDs, fall into two separate subpopulations, one of which has a much higher on-fraction than the other. We delineate a high on-fraction population (HOFP) and low on-fraction population (LOFP) as illustrated in Figure 2e. We observe that the LOFP results from some QDs exhibiting defects resulting in a drastic reduction in on-fraction. We analyzed Z-STEM images to compare the QDs inhabiting each population, allowing us to understand the distinct structural features that result in QD on-fraction segregation. All Z-STEM images for the 84 QDs studied herein are shown in Supporting Information Figure S3.

The Z-STEM images hold a wealth of information including size parameters, crystal structure, CdS shell epitaxy, and QD orientation. Additionally, contrast highlights variances in atomic composition, providing information about the shell epitaxy and core/shell interface.[40] Using this information in conjunction with observed lattice fringes and previous work[32,41] we determined which facets of the core were passivated by CdS and how much shell material was present for each QD. For the purposes of our discussion, because there is some overlap in the LOFP and HOFP, we established the cutoff at an on-fraction of 0.70. In all, 26 of the investigated QDs (31%) resided in the HOFP; these QDs exhibited both structural integrity and inorganic passivation of a large number of facets on the CdSe core by the CdS shell.

Probing the Effects of Internal and Surface Defects on Single Quantum Dots. The presented technique allowed us to directly correlate specific structural defects with decreased photoluminescence of individual QDs. We used the acquired data to understand the effect of three commonly encountered defects: (1) stacking faults within the core or the core/shell heterostructure, (2) unpassivated Cd-rich (101) core facets, and (3) an etched/unpassivated Cd-rich (001) core facet.

Out of the 84 QDs studied here, 12 were seen to exhibit highly visible zinc blende stacking faults. An example is shown in Figure 3. Our data show that stacking faults facilitate charge trapping and promote nonradiative decay, as indicated by an average on-fraction of 0.26 (n = 12). Previous work on II–VI semiconductor quantum wells has shown that stacking faults in the material act as efficient nonradiative recombination sites,[42] and it has been postulated that the same effect should be seen in QDs and QD heterostructures.[43] The stacking faults we observed were at the core/shell interface for 8 of 12 QDs (75%), indicating that this defect is likely formed during growth of the inorganic CdS shell onto the CdSe core.

Two morphological defect structures of individual QDs are shown in Figure 4. The first of these, pictured in Figure 4a, is a "pinched" shape that results from the presence of stoichiometrically distinct facets on the CdSe core:[44] the CdS shell grows preferentially onto the Se-rich (001) and chemically neutral (010) and (100) facets, in contrast with the ideal traditional concerted growth process that results in a contiguous shell.

The second morphological defect we took note of was the presence of a "divot" on the Cd-rich (001) surface of the QD core. This defect, which is shown in

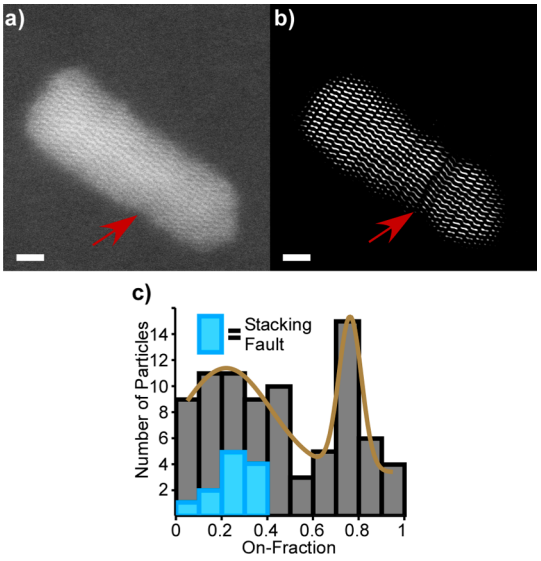

Figure 3. Characteristic defects for QDs with a low on-fraction. Shown in (a) is an example of a QD with a stacking fault. (b) The inverse Fourier transformed image demonstrates the disruption in the regular wurtzite lattice; (c) illustrates that all QDs with a similar visible stacking fault were observed in the LOFP. Scale bars are 2 nm.

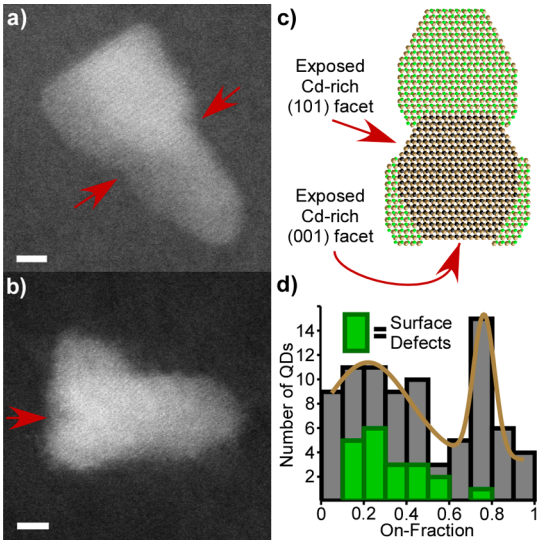

Figure 4. Characteristic defects for QDs with a low on-fraction. An example of a QD exhibiting a "pinched" shape is shown in (a), and an example of irregular shell growth at the base of a bullet QD is shown in (b). Highlighted on the representative QD structure in (c) are Cd-rich facets onto which lack of shell growth results in a lower on-fraction. These defects limit the on-fraction of QDs possessing them, as shown in the overlaid histogram in (d). Scale bars are 2 nm.

Figure 4b, arises due to uneven CdS shell growth: outgrowths from the Se-rich (101) facets result in the "divot" near the Cd-rich surface. This corresponds with the general trend that we observe—namely that incomplete coverage of Cd-rich facets produces QDs with a much lower on-fraction.

As shown in Figure 4c, the misshapen "pinched" and "divot" structures possess Cd-rich regions of the CdSe core that are exposed (not fully passivated), thereby increasing the likelihood of carrier trapping on the CdSe surface and lowering the observed on-fraction. QDs exhibiting an excessively exposed CdSe core, noncontiguous CdS shell growth, or some combination of these defects almost exclusively inhabit the LOFP, as shown in Figure 4d. The average on-fraction of QDs with these surface defects was 0.30 (n=31). All QDs meeting these criteria are highlighted in Supporting Information Figure S3.

The observed exposed Cd-rich core regions are not necessarily fully bare. Likely, there are passivating ligands on the surface of both the core and shell. These ligands, while effective at passivating some surface defects such as dangling bonds, are less photostable than an inorganic shell, and are not effective at eliminating vacancies at the surface of the core.[45] This can be seen by comparing the blinking behavior of QDs with no inorganic shell to nonblinking QDs with rationally designed gradient and thick inorganic shells.[23,24]

The traps formed at the surface of the CdSe core could be either shallow or deep surface traps due to vacancies, surface oxidation or dangling bonds.[46] In fact, it has recently been proposed that surface vacancies, if unpassivated, can atomically rearrange to transition from shallow to deep traps. This change would occur *via* charging of the QD, or even as a result of photoinduced surface rearrangement.[45,47] Our group has experimentally observed electron beam induced surface rearrangement, and similar results could be expected for single QD photoexcitation.[41,48]

For CdSe nanocrystals, shell material tends to favor nucleation and growth from the Se-rich (001) facet. The faceting of the wurtzite cores used for these commercial QDs results in the "bullet" shape observed in the QD population studied. Although this morphology is not ubiquitous, many core/shell syntheses display preferential shell growth onto chemically distinct core facets.[49] For this reason, the concepts introduced herein apply to many common literature preparation methods.

Quantum Dot Structures in the High On-Fraction Population. The collected data also allowed us to visualize the structures of QDs with high on-fractions in an effort to ascertain unifying characteristics within this population. Not surprisingly, the most commonly observed features were good structural integrity and near-complete inorganic passivation of the core. Two other less-expected features were observed as well.

Out of the 84 QDs studied, the QDs oriented on end, with the C_{3v} axis perpendicular to the substrate, were seen to reside in the HOFP (average on-fraction = 0.87, n = 3, Figure 5a). Z-STEM images show that, for these QDs, a large number of (010), (100) and corresponding facets are well passivated by CdS, resulting in high on-fractions. The reduced cumulative "off" time in these QDs may be further explained by a lack of interaction of the CdS shell surface with the SiO_2 substrate.[39]

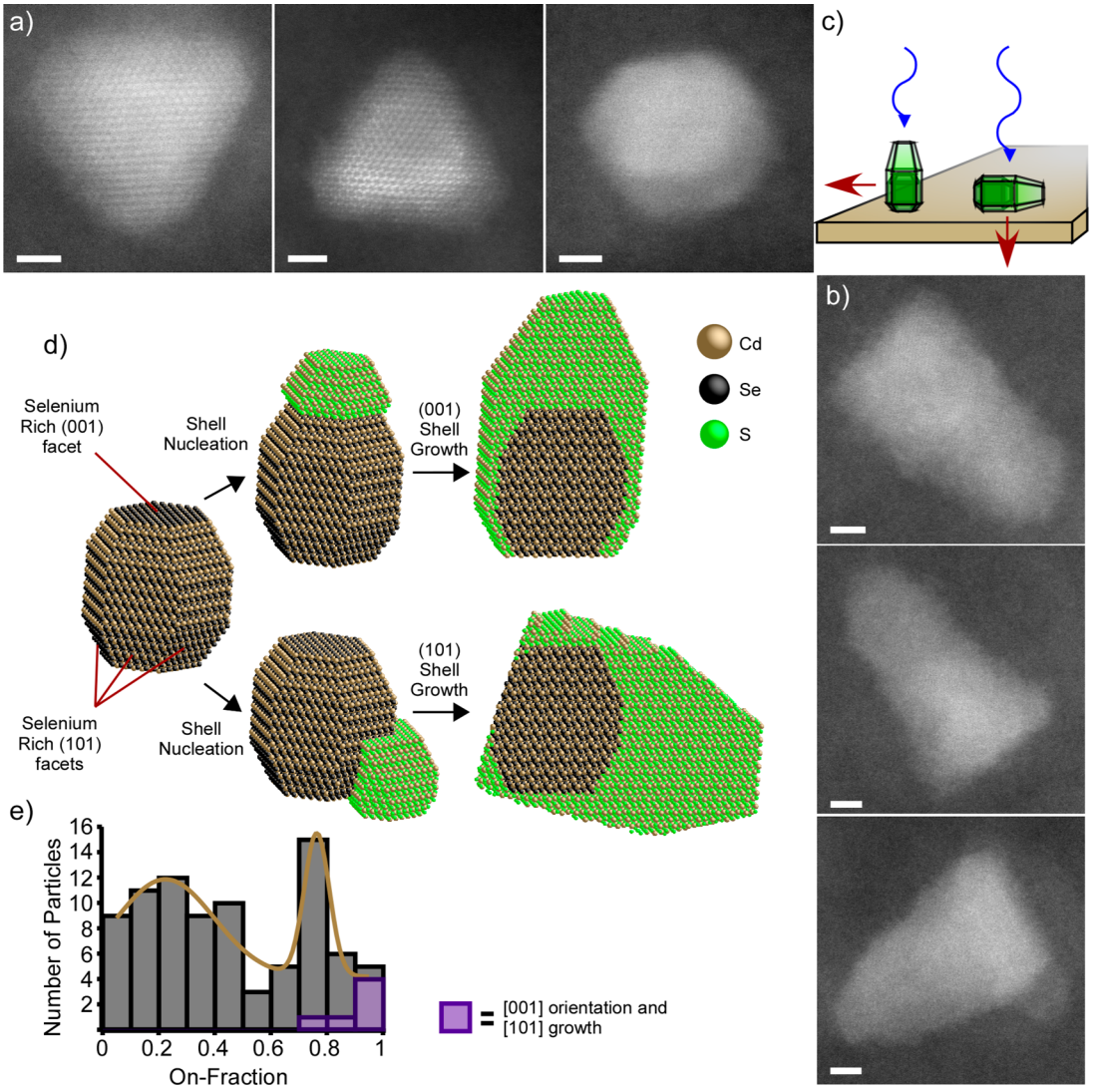

Figure 5. Structures of suppressed blinking QDs. The QD configurations with the highest on-fraction are shown in (a) and (b). Only three QDs were oriented along the *c*-axis (a), as shown on the left in (c); these QDs all exhibited highly suppressed blinking. All QDs but these three were oriented side-on, as shown on the right in (c). Also included in the high on-fraction population were QDs showing CdS shell growth from the Se-rich (101) face of the CdSe core (b). A cartoon of the previously unaddressed growth mechanism of these QDs is illustrated below the more common traditional growth in (d). The on-fraction distribution of these QDs with respect to all QDs in the sample demonstrates the suppressed blinking observed (e). Scale bars are 2 nm.

Further exploration of this orientation in the future will allow a more complete understanding of the high observed on-fraction.

Figure 5b highlights a subset of QDs with a high on-fraction that exhibit a previously unaddressed shell growth (average on-fraction = 0.89, $n = 3$). The lattice spacing and orientation of these QDs indicate that the view angle is along the [111] axis. In order for this structure to be formed, the CdS shell must nucleate and grow from a Se-rich (101) facet, as opposed to the commonly observed nucleation and growth from the Se-rich (001) facet. Although the traditional "bullet" shape is preserved, the lengthwise growth does not occur parallel to the C_{3v} axis of the CdSe core. This growth mechanism is highlighted in Figure 5d. Because the (101) facet is surrounded by two other Se-rich (101), one chemically neutral (010), and only one Cd-rich (001) facet,[44] shell growth after nucleation passivates a large area on the surface of the core. Specifically, this growth method seems to passivate the Cd-rich (001) facet, which is typically almost completely bare for the more common "bullet" shaped QDs, as seen in Figure 5d. We postulate that blinking may also be suppressed due to anisotropy between the core C_{3v} axis and the confining potential of the CdS shell.[50]

Determination of the Crystal Structure of Single Nonradiative Quantum Dots. One of the unique aspects of our approach is that it facilitates investigation of the structures of nonradiative, or "dark", QDs. In the total population, 7 of the 84 QDs observed *via* Z-STEM were labeled as "dark" QDs. Optical excitation of the "dark" QDs in the fluorescence microscope did not yield

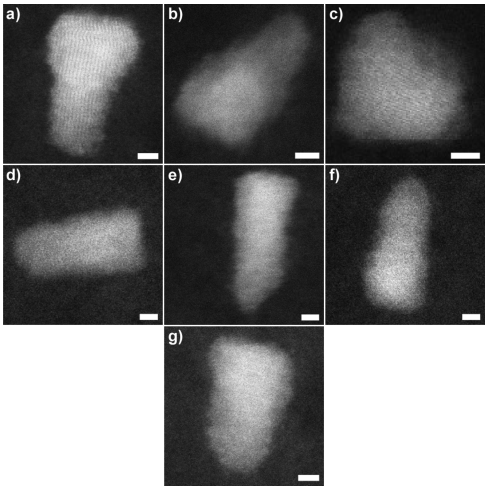

Figure 6. Structures of nonradiative QDs. Our technique affords the ability to determine the crystal structures of permanently nonradiative, or "dark", QDs. The seven "dark" QDs identified in this study are shown here. Scale bars are 2 nm.

fluorescence at any point during the collection period. The structures of these 7 QDs are shown in Figure 6.

Previous studies have identified the existence of permanently nonradiative QDs,[51,52] and it has been speculated that a permanently dark population may be the source of low PL quantum yield (PLQY) in nonblinking QDs.[26] Our ability to pinpoint and directly observe the atomic structures of these QDs is unmatched, however, and will allow a more complete understanding of the array of QDs that are detrimental to ensemble PLQY.

Examination of the "dark" QD structures reveals some interesting details. The QD shown in Figure 6a was the only QD in this study with a visible stacking fault in the core region. This may indicate the presence of a permanent internal defect at the core surface that results in a high rate of nonradiative recombination. The QD in Figure 6b shows a noncontiguous, asymmetric shell growth that would be expected to provide inefficient passivation for the same reasons outlined above for QDs in the LOFP. The QD shown in Figure 6c is anomalous in that it has little or no shell material grown onto the CdSe core. This QD would be excessively prone to surface oxidation and surface trap formation. The other "dark" QDs (Figure 6d–g) do not show egregious surface or internal defects. This indicates that perhaps there is some nonstructural explanation for a lack of PL in QDs. Future studies will add to the library of "dark" QD structures, and will allow us to determine any structural motif among these QDs.

CONCLUSIONS

The presented correlation technique allowed investigation of the fine structural factors that mediate QD PL. We were able to unambiguously pinpoint the effect of specific surface and internal defects on the PL of single CdSe/CdS core/shell QDs. We found that, for the investigated QDs, shell material often covers little to none of the Cd-rich (001) or (101) facets. This lack of complete coverage results in the "pinched" and "divot" morphologies that we observed to decrease the total radiative time in single QDs. We also observed that stacking faults at the core/shell interface are detrimental to efficient radiative recombination in individual QDs. We now have direct evidence of what has previously been suspected: Cd-rich surface sites act as physical trap sites and the presence of a stacking fault at the core/shell interface enhances nonradiative recombination.

We also observed that suppressed blinking in anisotropic QDs can arise due to both orientational and structural factors, as illustrated by the suppressed blinking observed for all QDs oriented with the C_{3v} axis perpendicular to the substrate. The correlation also identifies structures of QDs in the permanently nonradiative "dark" fraction; the information learned about these structures can be used to eliminate the "dark" QDs, thereby increasing ensemble PLQY. In the future, examination of heterogeneity within a population of isotropic QD heterostructures made with spherically faceted cores will be useful in further elucidating ideal structures for designer QD emitters.

Ultimately, our correlation technique can be expanded to determine the structure dependence of a vast array of optical parameters. These include single QD spectra, spectral diffusion,[53] biexciton quantum yield, blinking frequency, and both excitonic and biexcitonic PL lifetime. Polarization dependence of PL behavior can also easily be examined, as dipole orientation is readily identified *via* electron microscopy. We believe that the use of this correlated characterization tool will facilitate rapid synthetic enhancement of desired QD properties for less developed, emergent QD systems.

EXPERIMENTAL METHODS

Sample Preparation. Samples were prepared by spincasting polystyrene latex spheres (PS, Ted Pella, 1 μm) from a stock aqueous solution onto transmission electron microscopy (TEM) support films (Ted Pella, PELCO 8 nm Ultra-Flat Silicon Dioxide Support Film). After spincasting, the PS naturally group into random formations that are readily identifiable in both fluorescence images and scanning transmission electron micrographs. These formations acted as fiducial markers from which single QD locations could be surmised, as illustrated in Figure 7. Subsequent to PS deposition, 5 μL of a 100 pM aqueous QD solution was dropped on the support film; residual liquid was wicked away with a KimWipe. This sample preparation resulted in a density of ~0.0015 QDs/μm^2; this ensured single QDs were adequately spatially separated to avoid influence of QD–QD interactions.

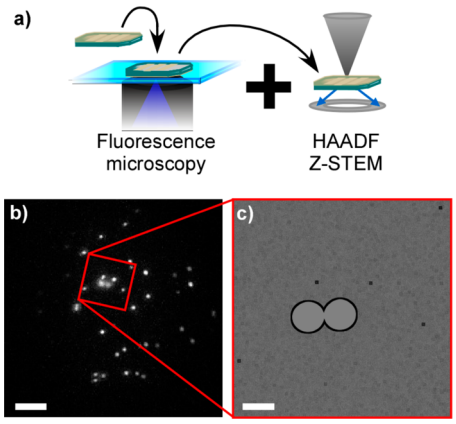

Figure 7. Correlation of optical and electron microscopy. (a) Correlation was achieved by loading an 8 nm SiO_2 support film on a windowed Si_3N_4 frame with polystyrene latex spheres and QDs. The grid was placed face down onto a coverslip to allow for optical imaging, and subsequently imaged in the electron microscope. (b) An image mapping the fluorescence maximum for each pixel over 100 s shows the location of QDs under wide-field optical excitation. (c) A filtered electron micrograph of the same QDs shown in (b); polystyrene latex spheres serve as fiducial markers. A post-processed maximum filter was utilized to make the location of the QDs more visible in the micrograph shown in (c). The correlation process is rigorously demonstrated in Supporting information Figures S1 and S2. Scale bar is 5 μm in (b) and 1 μm in (c).

Optical Microscopy. The optical setup is a modified version of that reported by Dukes *et al.*[54] A neodymium-doped yttrium orthovanadate (Nd:YVO_4) continuous-wave laser (Coherent Verdi, 532 nm, 18W) pumps a titanium sapphire (Ti:Al_2O_3) oscillator (Coherent, Mira 900 basic, 800 nm). The oscillator seeds a regenerative amplifier (Coherent, RegA 9000) that is used to drive an optical parametric amplifier (Coherent, OPA 9400). The frequency doubled output of the OPA 9400 is used in these experiments because it provides excitation at 400 nm and a pulse separation of 4 μs, thus ensuring that the QDs are able to fully relax between excitation events. The excitation beam passes through a neutral density filter and reflects from a series of mirrors before being expanded $\times$2 and focused by a 300 mm focal length lens to provide wide-field Köhler epi-illumination within a custom-built inverted microscope. The microscope uses a water immersion objective (Olympus, UPlanSApo 60$\times$, 1.2 N.A., ∞/0.13−0.21, FN 26.5). The excitation beam is linearly polarized and enters the objective off a 410 nm long-pass dichroic filter (Omega Optics, 3RD410LP) set for s-polarized reflection at an incidence angle of $\sim$10°. A 3D piezostage (ThorLabs, MAX301) and controller box (ThorLabs, BPC203) were used to lower the sample into position above the objective. Emitted fluorescence from the excitation area, was a disk of $\sim$100 μm diameter, was collected by the objective, passed through the dichroic and a 600 nm LP filter (ThorLabs, FEL0600) and is imaged onto an EM-CCD camera (Andor, iXonEM+, DU-897e-CSO-#BV) using an achromat tube lens with focal length of 250 mm and a 1:1 relay lens system, resulting in an optical magnification of 83.3. The neutral density filter was adjusted to limit irradiance in order to prevent multiple exciton generation.

Once the sample was prepared, the TEM support film was placed, facing downward, onto a No. 0 glass coverslip. The piezostage was maneuvered to bring the image on the EMCCD camera into focus. The focus was found by removing the Kohler lens and adjusting the piezo stage so that the laser beam focused at the coverslip and partially reflected back along the incident path. Polystyrene latex beads were used in conjunction with the border of the support film to allow for recording of positional information. The EM-CCD was cooled to −50 °C, and all videos were recorded at a frame resolution of 100 ms (refresh rate 0.1027 s) for 20 000 frames (2054 s). The illuminated portion of the sample was imaged onto a section of the camera with a diameter of $\sim$250 pixels. Electron-multiplying gain was set to 300$\times$ and pixels were binned 2 $\times$ 2, resulting in an image of 128 $\times$ 128 pixels with 0.384 μm/pixel in object space. An example of a typical wide-field fluorescent image is shown in Figure 1b.

Electron Microscopy. Scanning transmission electron microscopy images were obtained using a Tecnai Osiris operating at 200 kV, with a spot size set to 10 (to reduce charging effects) and a camera length of 220 mm for HAADF imaging. STEM-HAADF imaging was chosen over HRTEM imaging since the white-on-dark-contrast for STEM greatly facilitates the location of individual quantum dots at low magnifications. Patterns of polystyrene were used to align the STEM image and distances measured from the optical microscope were used to identify regions of interest. An example of a typical low-magnification electron micrograph is shown in Figure 7c. Large area images were used to identify neighboring particles and possible dark particles.

Data Analysis. The brightest pixel in a 2 $\times$ 2 pixel area in each frame was chosen and used to determine the transient for each QD. Very infrequently, STEM imaging would reveal the presence of multiple QDs in the same ROI from optical imaging. In this case, the ROI was not considered a part of the single QD population being probed. Custom LabView software was used to determine the following parameters for each QD according to the referenced literature methods: (a) on (off) times, (b) on (off) time probability distribution,[13] and (c) on (off) time memory parameters R(on), R(on)log, R(off), R(off)log.[55]

Conflict of Interest: The authors declare no competing financial interest.

Supporting Information Available: Supplementary Figures S1−S6, including full illustration of the correlation method and HAADF Z-STEM micrographs of the 84 QDs studied. Supplementary text is also included. This material is available free of charge *via* the Internet at http://pubs.acs.org.

Acknowledgment. The authors would like to acknowledge support from the National Science Foundation CHE grant 1213758 and National Science Foundation EPS 1004083 (TN-SCORE).

REFERENCES AND NOTES

1. Murray, C.; Kagan, C.; Bawendi, M. Synthesis and Characterization of Monodisperse Nanocrystals and Close-Packed Nanocrystal Assemblies. *Annu. Rev. Mater. Sci.* **2000**, *30*, 545–610.
2. Achermann, M.; Petruska, M.; Koleske, D.; Crawford, M.; Klimov, V. Nanocrystal-Based Light-Emitting Diodes Utilizing High-Efficiency Nonradiative Energy Transfer for Color Conversion. *Nano Lett.* **2006**, *6*, 1396–1400.
3. Anikeeva, P.; Halpert, J.; Bawendi, M.; Bulovic, V. Quantum Dot Light-Emitting Devices with Electroluminescence Tunable over the Entire Visible Spectrum. *Nano Lett.* **2009**, *9*, 2532–2536.
4. Caruge, J.; Halpert, J.; Wood, V.; Bulovic, V.; Bawendi, M. Colloidal Quantum-Dot Light-Emitting Diodes with Metal-Oxide Charge Transport Layers. *Nat. Photonics* **2008**, *2*, 247–250.
5. Kim, T.; Cho, K.; Lee, E.; Lee, S.; Chae, J.; Kim, J.; Kim, D.; Kwon, J.; Amaratunga, G.; Lee, S.; *et al.* Full-Colour Quantum Dot Displays Fabricated by Transfer Printing. *Nat. Photonics* **2011**, *5*, 176–182.
6. Pattantyus-Abraham, A.; Kramer, I.; Barkhouse, A.; Wang, X.; Konstantatos, G.; Debnath, R.; Levina, L.; Raabe, I.; Nazeeruddin, M.; Gratzel, M.; *et al.* Depleted-Heterojunction Colloidal Quantum Dot Solar Cells. *ACS Nano* **2010**, *4*, 3374–3380.
7. Meinardi, F.; Colombo, A.; Velizhanin, K.; Simonutti, R.; Lorenzon, M.; Beverina, L.; Viswanatha, R.; Klimov, V.; Brovelli, S. Large-Area Luminescent Solar Concentrators Based on 'Stokes-Shift-Engineered' Nanocrystals in a Mass-Polymerized PMMA Matrix. *Nat. Photonics* **2014**, *8*, 392–399.
8. Klimov, V.; Mikhailovsky, A.; McBranch, D.; Leatherdale, C.; Bawendi, M. Quantization of Multiparticle Auger Rates

in Semiconductor Quantum Dots. *Science* **2000**, *287*, 1011–1013.
9. Chen, J.; Hardev, V.; Yurek, J. Quantum-Dot Displays: Giving LCDs a Competitive Edge Through Color. http://static.squarespace.com/static/526856d7e4b05b8fbefaa9b6/t/52b129a9e4b05d40c788d84e/1387342249119/QDEF%20InformationDisplay.pdf (accessed 10/28/2014).
10. Chang, J.; Rosenthal, S. A Bright Light to Reveal Mobility: Single Quantum Dot Tracking Reveals Membrane Dynamics and Cellular Mechanisms. *J. Phys. Chem. Lett.* **2013**, *4*, 2858–2866.
11. Nirmal, M.; Dabbousi, B.; Bawendi, M.; Macklin, J.; Trautman, J.; Harris, T.; Brus, L. Fluorescence Intermittency in Single Cadmium Selenide Nanocrystals. *Nature* **1996**, *383*, 802–804.
12. Efros, A.; Rosen, M. Random Telegraph Signal in the Photoluminescence Intensity of a Single Quantum Dot. *Phys. Rev. Lett.* **1997**, *78*, 1110–1113.
13. Kuno, M.; Fromm, D.; Hamann, H.; Gallagher, A.; Nesbitt, D. Nonexponential "Blinking" Kinetics of Single CdSe Quantum Dots: A Universal Power Law Behavior. *J. Chem. Phys.* **2000**, *112*, 3117–3120.
14. Shimizu, K.; Neuhauser, R.; Leatherdale, C.; Empedocles, S.; Woo, W.; Bawendi, M. Blinking Statistics in Single Semiconductor Nanocrystal Quantum Dots. *Phys. Rev. B* **2001**, 63.
15. Cordones, A.; Leone, S. Mechanisms for Charge Trapping in Single Semiconductor Nanocrystals Probed by Fluorescence Blinking. *Chem. Soc. Rev.* **2013**, *42*, 3209–3221.
16. Jha, P.; Guyot-Sionnest, P. Trion Decay in Colloidal Quantum Dots. *ACS Nano* **2009**, *3*, 1011–1015.
17. Ye, M.; Searson, P. Blinking in Quantum Dots: The Origin of the Grey State and Power Law Statistics. *Phys. Rev. B* **2011**, *84*, 1253171–1253178.
18. Margolin, G.; Protasenko, V.; Kuno, M.; Barkai, E. Photon Counting Statistics for Blinking CdSe-ZnS Quantum Dots: A Levy Walk Process. *J. Phys. Chem. B* **2006**, *110*, 19053–19060.
19. Goushi, K.; Yamada, T.; Otomo, A. Excitation Intensity Dependence of Power-Law Blinking Statistics in Nanocrystal Quantum Dots. *J. Phys. Chem. C* **2009**, *113*, 20161–20168.
20. Kuno, M.; Fromm, D.; Hamann, H.; Gallagher, A.; Nesbitt, D. "On"/"Off" Fluorescence Intermittency of Single Semiconductor Quantum Dots. *J. Chem. Phys.* **2001**, *115*, 1028–1040.
21. Hines, M.; Guyot-Sionnest, P. Synthesis and Characterization of Strongly Luminescing ZnS-Capped CdSe Nanocrystals. *J. Phys. Chem.* **1996**, *100*, 468–471.
22. Keene, J. D.; McBride, J. R.; Orfield, N. J.; Rosenthal, S. J. Elimination of Hole-Surface Overlap in Graded CdSxSe1-x Nanocrystals Revealed by Ultrafast Fluorescence Upconversion Spectroscopy. *ACS Nano* **2014**, *8*, 10665–10673.
23. Chen, Y.; Vela, J.; Htoon, H.; Casson, J.; Werder, D.; Bussian, D.; Klimov, V.; Hollingsworth, J. "Giant" Multishell CdSe Nanocrystal Quantum Dots with Suppressed Blinking. *J. Am. Chem. Soc.* **2008**, *130*, 5026–5027.
24. Wang, X.; Ren, X.; Kahen, K.; Hahn, M.; Rajeswaran, M.; Maccagnano-Zacher, S.; Silcox, J.; Cragg, G.; Efros, A.; Krauss, T. Non-Blinking Semiconductor Nanocrystals. *Nature* **2009**, *459*, 686–689.
25. Park, Y.; Bae, W.; Padilha, L.; Pietryga, J.; Klimov, V. Effect of the Core/Shell Interface on Auger Recombination Evaluated by Single-Quantum-Dot Spectroscopy. *Nano Lett.* **2014**, *14*, 396–402.
26. Ghosh, Y.; Mangum, B.; Casson, J.; Williams, D.; Htoon, H.; Hollingsworth, J. New Insights into the Complexities of Shell Growth and the Strong Influence of Particle Volume in Nonblinking "Giant" Core/Shell Nanocrystal Quantum Dots. *J. Am. Chem. Soc.* **2012**, *134*, 9634–9643.
27. Zhao, J.; Chen, O.; Strasfeld, D.; Bawendi, M. Biexciton Quantum Yield Heterogeneities in Single CdSe (CdS) Core (Shell) Nanocrystals and Its Correlation to Exciton Blinking. *Nano Lett.* **2012**, *12*, 4477–4483.
28. Lidke, K.; Rieger, B.; Jovin, T.; Heintzmann, R. Superresolution by Localization of Quantum Dots Using Blinking Statistics. *Opt. Express* **2005**, *13*, 7052–7062.
29. Wang, Y.; Fruhwirth, G.; Cai, E.; Ng, T.; Selvin, P. 3D Super-Resolution Imaging with Blinking Quantum Dots. *Nano Lett.* **2013**, *13*, 5233–5241.
30. Koberling, F.; Mews, A.; Philipp, G.; Kolb, U.; Potapova, I.; Burghard, M.; Basche, T. Fluorescence Spectroscopy and Transmission Electron Microscopy of the Same Isolated Semiconductor Nanocrystals. *Appl. Phys. Lett.* **2002**, *81*, 1116–1118.
31. Koberling, F.; Kolb, U.; Philipp, G.; Potapova, I.; Basche, T.; Mews, A. Fluorescence Anisotropy and Crystal Structure of Individual Semiconductor Nanocrystals. *J. Phys. Chem. B* **2003**, *107*, 7463–7471.
32. McBride, J.; Kippeny, T.; Pennycook, S.; Rosenthal, S. Aberration-Corrected Z-Contrast Scanning Transmission Electron Microscopy of CdSe Nanocrystals. *Nano Lett.* **2004**, *4*, 1279–1283.
33. Alivisatos, A. Perspectives on the Physical Chemistry of Semiconductor Nanocrystals. *J. Phys. Chem.* **1996**, *100*, 13226–13239.
34. Empedocles, S.; Neuhauser, R.; Shimizu, K.; Bawendi, M. Photoluminescence from Single Semiconductor Nanostructures. *Adv. Mater.* **1999**, *11*, 1243–1256.
35. Vanmaekelbergh, D.; Casavola, M. Single-Dot Microscopy and Spectroscopy for Comprehensive Study of Colloidal Nanocrystals. *J. Phys. Chem. Lett.* **2011**, *2*, 2024–2031.
36. Mangel, S.; Aronovitch, E.; Enyashin, A.; Houben, L.; Bar-Sadan, M. Atomic-Scale Evolution of a Growing Core-Shell Nanoparticle. *J. Am. Chem. Soc.* **2014**, *136*, 12564–12567.
37. Dickson, R. Structure Determines Function in Nanoparticles, Their Interfaces, and Their Assemblies. *J. Phys. Chem. Lett.* **2011**, *2*, 2044–2045.
38. Fernee, M.; Plakhotnik, T.; Louyer, Y.; Littleton, B.; Potzner, C.; Tamarat, P.; Mulvaney, P.; Lounis, B. Spontaneous Spectral Diffusion in CdSe Quantum Dots. *J. Phys. Chem. Lett.* **2012**, *3*, 1716–1720.
39. Krasselt, C.; Schuster, J.; von Borczyskowski, C. Photoinduced Hole Trapping in Single Semiconductor Quantum Dots at Specific Sites at Silicon Oxide Interfaces. *Phys. Chem. Chem. Phys.* **2011**, *13*, 17084–17092.
40. McBride, J.; Treadway, J.; Feldman, L.; Pennycook, S.; Rosenthal, S. Structural Basis for Near Unity Quantum Yield Core/Shell Nanostructures. *Nano Lett.* **2006**, *6*, 1496–1501.
41. McBride, J.; Pennycook, T.; Pennycook, S.; Rosenthal, S. The Possibility and Implications of Dynamic Nanoparticle Surfaces. *ACS Nano* **2013**, *7*, 8358–8365.
42. Guha, S.; DePuydt, J. M.; Qiu, J.; Hofler, G. E.; Haase, M. A.; Wu, B. J.; Cheng, H. Role of Stacking-Faults as Misfit Dislocation Sources and Nonradiative Recombination Centers in II-VI Heterostructures and Devices. *Appl. Phys. Lett.* **1993**, *63*, 3023–3025.
43. Guyot-Sionnest, P.; Hines, M. Intraband Transitions in Semiconductor Nanocrystals. *Appl. Phys. Lett.* **1998**, *72*, 686–688.
44. Taylor, J.; Kippeny, T.; Rosenthal, S. Surface Stoichiometry of CdSe Nanocrystals Determined by Rutherford Backscattering Spectroscopy. *J. Cluster Sci.* **2001**, *12*, 571–582.
45. Voznyy, O.; Sargent, E. Atomistic Model of Fluorescence Intermittency of Colloidal Quantum Dots. *Phys. Rev. Lett.* **2014**, 112.
46. Lifshitz, E.; Dag, I.; Litvitn, I.; Hodes, G. Optically Detected Magnetic Resonance Study of Electron/Hole Traps on CdSe Quantum Dot Surfaces. *J. Phys. Chem. B* **1998**, *102*, 9245–9250.
47. Voznyy, O.; Thon, S.; Ip, A.; Sargent, E. Dynamic Trap Formation and Elimination in Colloidal Quantum Dots. *J. Phys. Chem. Lett.* **2013**, *4*, 987–992.
48. Pennycook, T.; McBride, J.; Rosenthal, S.; Pennycook, S.; Pantelides, S. Dynamic Fluctuations in Ultrasmall Nanocrystals Induce White Light Emission. *Nano Lett.* **2012**, *12*, 3038–3042.
49. Rosenthal, S.; McBride, J.; Pennycook, S.; Feldman, L. Synthesis, Surface Studies, Composition and Structural Characterization of CdSe, Core/Shell and Biologically Active Nanocrystals. *Surf. Sci. Rep.* **2007**, *62*, 111–157.

50. Gomez-Campos, F.; Califano, M. Hole Surface Trapping in CdSe Nanocrystals: Dynamics, Rate Fluctuations, and Implications for Blinking. *Nano Lett.* **2012**, *12*, 4508–4517.
51. Ebenstein, Y.; Mokari, T.; Banin, U. Fluorescence Quantum Yield of CdSe/ZnS Nanocrystals Investigated by Correlated Atomic-Force and Single-Particle Fluorescence Microscopy. *Appl. Phys. Lett.* **2002**, *80*, 4033–4035.
52. Pons, T.; Medintz, I.; Farrell, D.; Wang, X.; Grimes, A.; English, D.; Berti, L.; Mattoussi, H. Single-Molecule Colocalization Studies Shed Light on the Idea of Fully Emitting *versus* Dark Single Quantum Dots. *Small* **2011**, *7*, 2101–2108.
53. Neuhauser, R.; Shimizu, K.; Woo, W.; Empedocles, S.; Bawendi, M. Correlation Between Fluorescence Intermittency and Spectral Diffusion in Single Semiconductor Quantum Dots. *Phys. Rev. Lett.* **2000**, *85*, 3301–3304.
54. Dukes, A.; Samson, P.; Keene, J.; Davis, L.; Wikswo, J.; Rosenthal, S. Single-Nanocrystal Spectroscopy of White-Light-Emitting CdSe Nanocrystals. *J. Phys. Chem. A* **2011**, *115*, 4076–4081.
55. Volkan-Kacso, S.; Frantsuzov, P.; Janko, B. Correlations between Subsequent Blinking Events in Single Quantum Dots. *Nano Lett.* **2010**, *10*, 2761–2765.